Article

Not peer-reviewed version

Computational Fluid Dynamic Optimization of Micropatterned Surfaces: Towards Biofunctionalization of Artificial Organs

Wenxuan He , Aminat M. Ibrahim , Abhishek Karmakar , Shivani Tuli , Jonathan Butcher , James F. Antaki *

Posted Date: 2 October 2024

doi: 10.20944/preprints202410.0108.v1

Keywords: LVAD; mechanical valves; thrombosis; endothelial cells; hemocompatibility; Mechanical devices

Article

Computational Fluid Dynamic Optimization of Micropatterned Surfaces: Towards Biofunctionalization of Artificial Organs

Wenxuan He [1], Aminat M. Ibrahim [2], Abhishek Karmakar [2], Shivani Tuli [2], Jonathan Butcher [2], and James F. Antaki [2,*]

[1] Sibley School of Mechanical and Aerospace Engineering, Cornell University, Ithaca, NY; wh444@cornell.edu
[2] Meinig School of Biomedical Engineering, Cornell University, Ithaca, NY
* Correspondence: antaki@cornell.edu

Abstract: Modifying surface topography to prevent surface-induced thrombosis in cardiovascular implants allows endothelialization, which is the natural thrombo-resistance of the blood-contacting surfaces and is deemed to be the only long-term hemocompatible material. We have adapted a simulation framework to predict platelet deposition on the modified surface and developed an optimization strategy to promote endothelial retention and limit platelet deposition. Under supraphysiological bulk shear stress, a maximum of 79% linear coverage was achieved. This study concludes that the addition of microtrenches promotes endothelial retention and can be improved through optimal selection of geometric parameters.

Keywords: LVAD; mechanical valves; thrombosis; endothelial cells; hemocompatibility; mechanical devices

1. Introduction

Artificial biomaterials contacting blood are widely used in implantable cardiovascular devices, including heart valves and left ventricular assist devices (LVADs). A significant challenge in the application of artificial biomaterials is surface-induced thrombosis, which results from protein adsorption, platelet adhesion, and activation [1,2]. Therefore, long-term coagulation management is required. However, this comes with its own risks, primarily an increased chance of hemorrhage [3]. Research indicates that patients with mechanical prosthetic heart valves face a significant risk of bleeding or clotting, with an accumulated risk as high as six percent per patient-year [4]. A report on patients with advanced heart failure who were treated with HeartMate 3 LVAD presented major bleeding events of 0.61 per patient-year, the greatest among all major adverse events [5].

This phenomenon starts with circulating plasma protein absorption on blood-contacting artificial material surface -- smaller proteins like human serum albumin, followed by larger proteins such as fibrinogen [6]. The adsorbed fibrinogen provides binding sites for platelets, which then become activated and release factors that promote further platelet aggregation and coagulation [7]. The foreign surface can also activate the intrinsic coagulation pathway through contact activation of Factor XII, leading to thrombin generation and fibrin formation [6,7]. This combination of activated platelets and the coagulation cascade results in the formation of a thrombus on the blood-wetted surfaces.

In contradistinction, endothelial cells (ECs) provide the natural thrombo-resistant lining of the blood-contacting surface and are deemed to be the only long-term hemocompatible material [8,9]. Healthy ECs utilize pathways such as the ecto-ADPase/CD39/NTPDase pathway, which limits the propagation of platelet activation and reduces the risk of thrombus formation; and the PGI2 and Nitric Oxide (NO) pathways, which inhibits platelet activation and aggregation through the stimulation of cAMP and cGMP production, respectively [10].

Therefore, there is a clear benefit to endothelialize cardiovascular implants [6,11]. One method of promoting endothelialization is through surface modification processes [12]. For instance, surfaces

 doi:10.20944/preprints202410.0108.v1

covered with microspheres (aka. sintering) are currently used in left ventricular assist devices (LVADs) [13]. Such sintered surface topography is adopted in the hope of growing neointima tissue and a continuous endothelium lining to shield the artificial surface from direct contact with blood, ultimately reducing surface thrombogenicity [13,14]. Unfortunately, studies published over the decades indicate that surface sintering can lead to unpredictable results, hence it is not a reliable method to avoid thromboembolism [13]. A critical limiting factor is the supraphysiological wall shear stress (WSS) commonly occurring in medical devices [15,16]. This limits endothelial attachment, and causes embolization. For example, the typical WSS associated with mechanical valve leaflets can range from 250 to 750 dynes/cm^2 [17,18], far in excess of the normal WSS in blood vessels (less than 50 dynes/cm^2) that allows endothelium to maintain its monolayer structure and perform its anticoagulation function [16].

Previous studies have shown that creating groove-like surface topography, named "microtrenches," can enhance EC retention in a supraphysiological shear environment, and consequently reduce platelet adhesion [17,19–24]. The underlying mechanism is that trenches create one or more vortices that attenuate WSS to a level tolerable for ECs. Daxini et al. created a grooving pattern of 32 μm deep and 35°, lowering WSS by 23% which helped to promote EC wound recovery [22]. To work with the shear range above 500 dynes/cm^2, Frendl et al. created several fold deeper trenches in pyrolytic carbon [23]. Therefore, the modified surface encouraged EC retention, inducing the release of anticoagulant molecules (e.g., nitric oxide) and reducing platelet adhesion greatly [23]. The efficacy of "microtrenches" was demonstrated to provide EC protection for over 48 hours of perfusion [23]. One of the objectives of the present study is to perform numerical simulations of these experimental results and further optimize the dimensions of the microtrench to maximize EC coverage. This is achieved by coupling automatic optimization software CAESES® (Friendship Systems AG, Potsdam, Germany) with the open-source CFD toolkit OpenFOAM.

2. Materials and Methods

2.1. Flow Field Simulation and Optimization of the Microtrenches

Numerical optimization of blood flow over a biomaterial surface populated with a series of microtrenches was performed. The computational domain consisted of a parallel plate channel with a height of 0.02" (~0.508 mm). The primary geometric variables of the trenches were: height (h) width (w) and draft angle (θ) of the walls, and gaps (d) therebetween. For all simulations, a constant velocity was specified at the inlet corresponding to the experimental procedure. The blood flow was modeled as a homogeneous Newtonian fluid governed by the Navier-Stokes equations. The corresponding Reynolds number is 83.2, therefore the flow was assumed to be laminar. The viscosity and density of the blood were specified as 3.5 cP and 1050 kg m^{-3} respectively. A previously validated multi-constituent thrombosis model [25] was applied to simulate the anticoagulant effect of the endothelial cell (EC) covered surface. The presence of the endothelial layer was modeled by altering the reaction rate that controls the flux of activated platelets to the surface.

We conduct a fully automatic optimization using parametric CFD optimization of the design variables. The geometric variables were provided by CAESES coupled with OpenFOAM. The objective function was the fraction of the projected area having WSS within the range of 10-50 dynes/cm^2.

$$f = \oint (A_{WSS} \cdot \vec{n}) / \oint (A_{trench} \cdot \vec{n}) \tag{1}$$

$$A_{WSS} = \begin{cases} A_{trench}, & if\ 10 < \tau < 50 \\ 0, & otherwise \end{cases} \tag{2}$$

where $\vec{n}$ is the normal vector of the surface, A_{trench} is the incremental surface area, $\oint (A_{WSS} \cdot \vec{n})$ is the projected cumulative area, τ is wall shear stress in dynes/cm^2.

These thresholds were chosen based on physiological WSS values and in vitro results proven to maintain EC monolayer integrity [16]. Additional constraints were applied, summarized in Table 1.

 doi:10.20944/preprints202410.0108.v1

The matrix of the combined effect of these three parameters is illustrated in Figure S1. Each parameter can pick one of three values, which yields 27 designs in total. The indices H1A1W1 refers to the smallest height, angle, and width, respectively.

Table 1. Design Space for trapezoidal microtrenches.

Design Variables	Lower Bound	Upper Bound	Average Interval
Height (mm)	0.01	3	0.1
Width (mm)	0.01	3	0.1
Angle*(°)	0	90	0.3

* Angle here is half of draft angle θ.

3. Results

3.1. Simulation of Platelet Adhesion

Initial simulations were conducted to mimic the published in-vitro experimental results of Frendl et al. [23]. Human endothelial cells seeded within collagen-coated microtrenches were exposed to a bulk shear stress of 600 dynes/cm², and human platelets afterward. The dimensions of the microtrenches were 700 μm deep and 400 μm wide.

The simulation employed a 2D domain corresponding to a channel with a fixed height with the bottom surface featuring 3 trenches (Figure 1 (a)). The domain includes sections of active collagen-coated surfaces and inactive surfaces pre-seeded with ECs. At the inlet, a uniform velocity was applied to achieve a wall shear stress of 600 dynes/cm² within the entrance length (and upper surface.) Figure 1 (b) shows that the wall shear stress distribution within the microtrench region was reduced by two orders of magnitude. The reduction of WSS was most dramatic within the microtrenches but the shear along the top of the partitions elevated WSS by approximately 60%.

The results of the multi-constituent thrombosis model are provided in Figure 1 (c) revealing that collagen-coated microtrenches yield noticeable thrombus formation inside the microtrenches at the time point of 50 minutes. The assumed 100% EC-coated microtrenches (Figure 1 (d)) in contrast were confirmed to limit platelet adhesion—corresponding to the experimental results (Frendl et al.), Figure 1 (e) demonstrating confluent ECs (red dots) retained on the microtrenched surface after 48 hours of perfusion and the absence of platelets (green dots) on microtrenched surfaces.

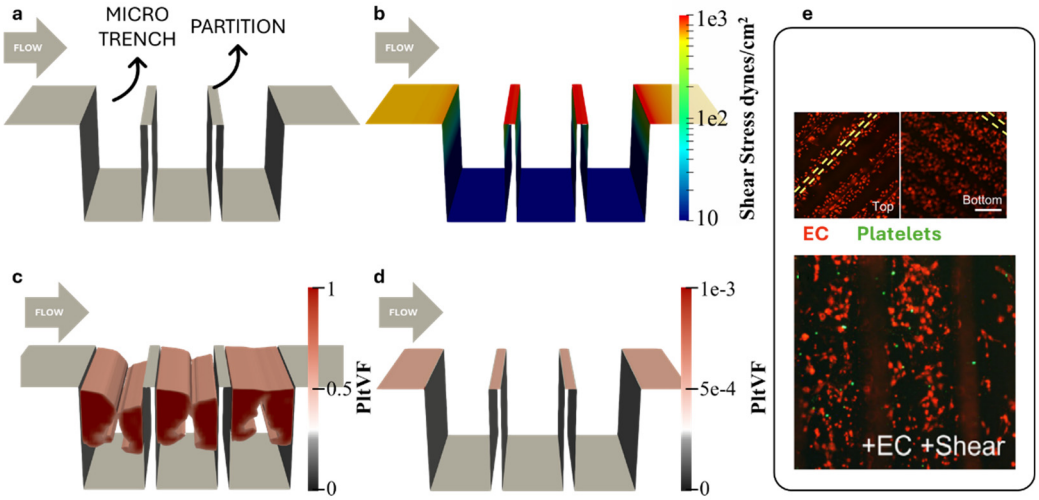

Figure 1. CFD and thrombosis simulation of vertical microtrench patterned surface. (a) Simulation domain. (b) Wall shear stress. (c) Simulation of thrombus within collagen-coated microtrenches at t = 3001. (d) no thrombus formation on EC-coated microtrenches; (e) Confluent EC (red) are retained after 48 h of 600 dyn/cm² steady bulk flow and images of platelets (green) adhesion to EC coated microtrenches surface. (Yellow dash lines indicate partition.) [23].

Preprints.org (www.preprints.org) | NOT PEER-REVIEWED | Posted: 2 October 2024 doi:10.20944/preprints202410.0108.v1

3.2. Optimization of Microtrenches

Figure 2 (a) provides a schematic of the initial geometry, corresponding to Friendl et al. [23] and (b) illustrates a generalized geometry in which the height (h), angle (θ), and width (w) are free variables, and the wall thickness is allowed to vanish to zero. Typical streamlines within the trenches, as shown in Figure 2 (c) and Figure 2 (d), reveal the presence of vortex formations.

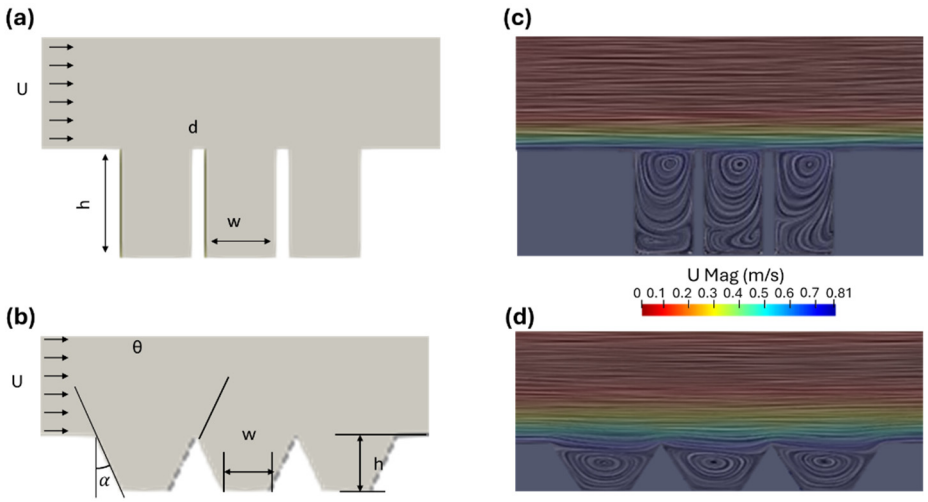

Figure 2. Overview of the geometry parameters and flow dynamics around different trench geometries. (a) Visualization of the vertical trench geometry. (b) Streamlines around the vertical trench, color-coded by velocity magnitude. (c) Flow patterns around a trapezoidal trench. (d) Streamlines around the trapezoidal trench, color-coded by velocity magnitude.

3.3. Optimization of Trapezoidal Trench Geometry

The optimization of microtrenches geometries is based on the evaluation of the coverage of the area with WSS ranging from 10 dynes/cm² to 50 dynes/cm². It can be seen in Figure 3 (a)-(c), that the WSS at the bottom corners of the microtrenches is less than 10 dynes/cm², as seen previously in Figure 1 (b) the bottom surface and hence is not optimal for maintaining EC monolayer integrity.

A pilot study in which the draft angle θ was varied from 60°, 90°, to 120° revealed a drastic variance in the profile of areas with desirable WSS, indicating that the angle has a significant impact on the WSS distribution and hence limits undesirable WSS bands. A quantitative comparison of coverage with a fixed height of 150 μm and width of 110 μm revealed that the right-angle microtrenches exhibited the most favorable WSS distribution, compared to 60° and 120° configurations. See Figure 3 (d).

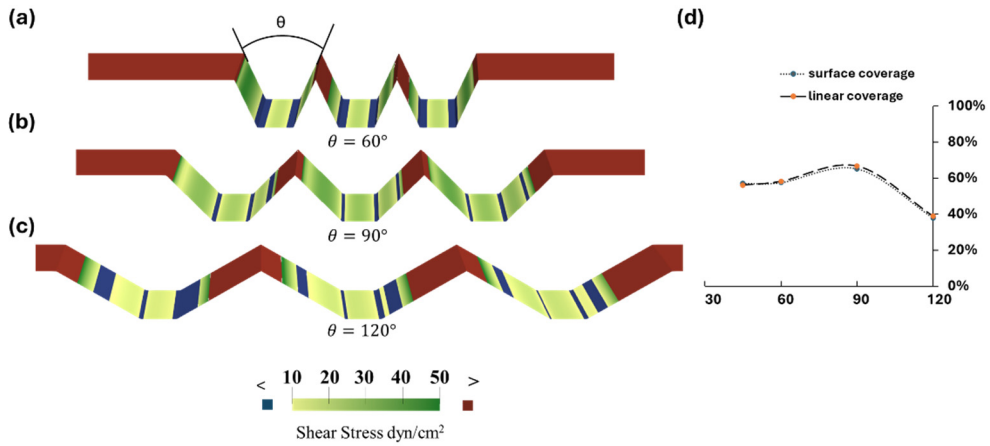

 doi:10.20944/preprints202410.0108.v1

Figure 3. (a)-(c) Evaluation of WSS on trapezoidal trenches with varying angles from 60° to 120°. The color-coding indicates areas with WSS values: green represents WSS within the threshold range of 10–50 dyn/cm², red denotes areas above 50 dyn/cm², and blue represents areas below 10 dyn/cm². (d) Surface coverage of the optimal WSS regions, along with the projected area coverage for comparative analysis across the designs.

An auto-optimization was conducted to identify the optimal combination of design parameters—draft angle (θ), height (h), and width (w)—to maximize the objective function. Figure 4 shows their effect on the objective function. The optimal configuration consisted of a trench height of 0.79 mm, a width of 1.6 mm, and a draft angle of 51.8°. However, as shown in Figure 4 (c), it is interesting to note that the width of the trench does not exhibit a direct correlation with the objective function, where no optimized value was found in this search.

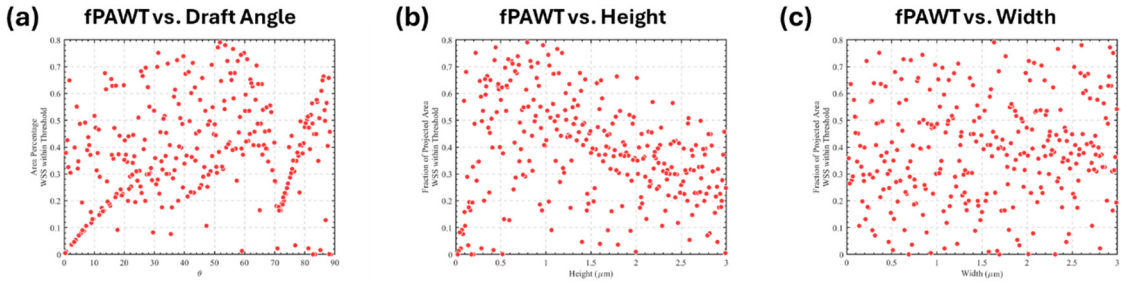

Figure 4. Exploration of design parameters and their influence on the projected area coverage. (a) Angle. (b) Height. (c) Width.

4. Discussion

This study presented a framework for optimizing the surface topography to promote endothelial cell retention and improve biocompatibility of implantable medical devices. Specifically, this study sought to optimize a trench-shaped surface topography under a single ultra-high shear environment, representative of the condition in devices such as mechanical prosthetic heart valves and inflow cannula of ventricular assist devices.

The optimization process began with pre-validated vertical microtrenches, investigating how the variation in the trench dimensions (height, width, and gaps) could influence the WSS profile and subsequently influence the EC coverage. However, the EC coverage achieved with this design was limited. The rationale for transitioning from vertical to trapezoidal trenches was twofold. Firstly, we observed that decreasing the gap between the vertical trenches did not result in a significant alteration of the WSS distribution inside the trench, as shown in Figure S2, yet the partition between two trenches is guaranteed to have undesirable high shear. This finding motivated us to reduce the gap further to increase the EC coverage while maintaining the mechanical integrity of the topography. Secondly, although the WSS on the vertical trench can be optimal, it failed to increase the projected EC coverage on a limited area of surface.

It is worth noting that a few assumptions were made thence the key simplifications have been applied for computing at a reasonable expense yet achieving realistic results. First, we assumed a 2D parallel plate channel which was chosen to be consistent with the in vitro validation experiment. Second, a uniform inlet velocity was introduced, and an ample entrance length allowed for the flow field to become fully developed at the leading edge of the trench. Third, we applied a steady-state flow instead of the pulsatile blood flow, which does not account for the complexity of the flow in vivo. This simulation also does not account for biological responses beyond the initial interaction of platelet deposition. The behavior of endothelial cells and thrombosis formation could vary under different flow conditions, including endothelial cell migration, mitosis, and or the secretion of anti-thrombotic substances in response to the shear stress.

Future studies should address these limitations by incorporating the cellular interaction between the endothelium and the blood, the secretion and transport of the anti-thrombotic substances, and its effect

 doi:10.20944/preprints202410.0108.v1

on platelet activation and aggregation. Such a model could also be applied in complex flow conditions, e.g., pulsatile flow, to represent the physiological environment; and more complex geometries.

The width of the trenches was examined as a parameter that could not be optimized within the constraints of the study. It is illustrated through an extreme case, where the microtrenches are reduced to a parallel plate. See Figure S3. Ideally, the wall shear stress is governed by the total height of the flow as explained in Equation (3):

$$\tau \propto \frac{1}{h_{total}} \tag{3}$$

where τ represents the wall shear stress, h_{total} is the total height of the channel without trenches. We hypothesize that there exists a critical height of the channel (10.952 mm) so that the WSS equals the desired threshold (10 dynes/cm^2). To validate this mathematical interpretation, we set the height at the critical value and compared the projected area coverage with varying channel widths. Results show that the objective function approaches an asymptotic value while the w extends to infinity. See Figure S3. This might result in an optimized design that has a width at the upper bound, such a value lacks practical meaning. In reality, the width of the trench is constrained by manufacturing limitations, mechanical stability, and other factors. Though it is not directly optimized, its selection is still guided by practical applications. Nevertheless, the addition of microtrenches will promote endothelial retention and can be improved through optimal selection of geometric parameters.

As a proof of concept of our optimized geometry, we evaluated endothelial retention on the trapezoidal microtrench by embossing a 45° trapezoidal geometry (shown using fluorescence image in Figure 5 (d) on a polymeric substrate. We then coated the embossed channel with collagen and seeded the channels with endothelial cells. CFD simulation Figure 5 (a) determined that the ECs experienced a shear range about 5-fold less than the applied bulk shear (120 dyn/cm^2), which supports the throttling capacity of the trapezoidal microtrench. Also, we found that the trench surface provided three times the surface area (Upstream, Base, and Downstream) in comparison to flat control, effectively increasing the surface area for EC adhesion. Twenty-four hours post-seeding, we applied continuous shear at a maximum pump flow rate for 48 hours. Endothelial retention on the flat microtrench control was completely diminished as shown in Figure 5 (b). However, we found a retained, confluent EC monolayer with visible junction integrity in the Upstream (U), Base(B), and Downstream (D) regions of the no-flow control microtrench (Figure 5 (c)) and sheared sample microtrench (Figure 5 (e)). Immunofluorescence staining showed expressed endothelial cell junction as marked by VE Caherin stain (CD144 monoclonal antibody, Bio-Rad, United States). Although comparable, we observed significant differences in endothelial coverage area fraction between the different regions of the sheared microtrench (84%, 87%, and 82%) vs. control (74%, 77%, and 69%) as shown in Figure 5 (f).

The above validates endothelial retention in the optimized trapezoidal microtrench under high shear stress, as ECs remain adhered to the microtrench channel, similar to Frendl et al. [23]. The downstream region in sheared samples showed higher degradation, which can be attributed to the force of fluid against the downstream wall. Furthermore, the endothelial retention rate corroborates our CFD optimization as we observed above 50% retention rate at the different regions within the microtrench post-shear, thus alluding to its potential to support more EC segments for monolayer formation. Although the height, width, and angle used in this experiment vary from the optimized geometry and cell culture medium was adopted to assess the long-term retention of the ECs, the results of EC retention on such microtrench were encouraging regarding the feasibility of seeding and the protection of the EC monolayer. In the future, we plan to address the difference between the simulation and the experiment and examine the effect of anti-platelet on the EC-coated microtrenches by incorporating blood as a fluid medium.

 doi:10.20944/preprints202410.0108.v1

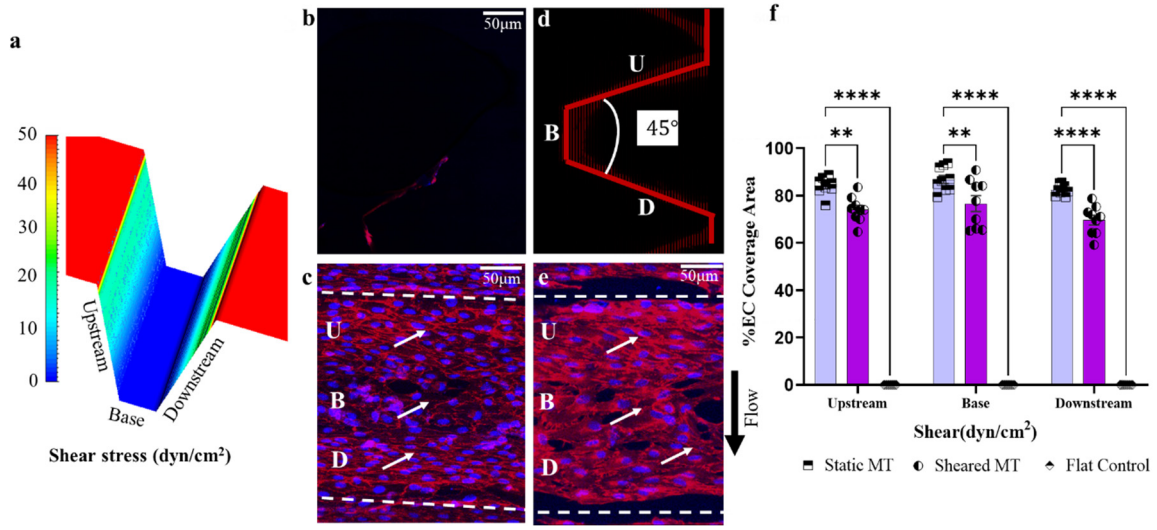

Figure 5. Endothelial retention under high shear stress. (a) CFD Simulation of trapezoidal microtrench (MT) at high pump flow rate; b. Immunohistochemistry images of the MT showing seeded endothelial cells. Flat MT control (b), Static MT with no flow (c), 3D projection of Sheared MT (d), Sheared MT at 48 hours post high shear (e). The arrows show mature endothelial junction, Blue (DAPI), Red (VE Cadherin). U, B, and D correspond to the Upstream, Base, and Downstream regions; (f) Quantification of EC Coverage at the different regions. Data represent mean ± SEM. n represents the number of independent biological samples with triplicates measured per sample. Two-way ANOVA with Tukey's HSD test. **** p = p < 0.0001; *** p = p < 0.0005; ** p = p < 0.005; * p = p < 0.05; ns = p > 0.05.

Supplementary Materials: The following supporting information can be downloaded at the website of this paper posted on Preprints.org, Figure S1: Visualization of 27 design configurations based on combinations of three design parameters: height (H), draft angle (A), and width (W). Figure S2: Comparison of shear stress distribution on the surface of two trenches with different gap widths (d). Figure S3: Exploration of an extreme design case.

Author Contributions: Conceptualization, W.H. and J.F.A.; methodology, W.H., A.M.I., and A.K.; software, W.H. and A.K.; validation, W.H.; formal analysis, W.H.; investigation, W.H.; resources, J.F.A. and J.B.; data curation, W.H.; writing—original draft preparation, W.H., A.M.I., and S.T.; writing—review and editing, A.K., J.B., and J.F.A.; visualization, W.H. and A.M.I.; supervision, J.B. and J.F.A.; project administration, J.F.A.; funding acquisition, J.F.A. All authors have read and agreed to the published version of the manuscript.

Funding: This research was funded by National Institute of Health, grant number HL089456.

Institutional Review Board Statement: Not applicable.

Informed Consent Statement: Not applicable.

Data Availability Statement: The original data presented in the study are available from the corresponding author, Dr. James F Antaki [antaki@cornell.edu].

Conflicts of Interest: The authors declare no conflicts of interests.

References

1. Gorbet, M.B.; Sefton, M. V Biomaterial-Associated Thrombosis: Roles of Coagulation Factors, Complement, Platelets and Leukocytes. In *The Biomaterials: Silver Jubilee Compendium*; 2006; Vol. 25, pp. 219–241 ISBN 9780080451541.
2. Labarrere, C.A.; Dabiri, A.E.; Kassab, G.S. Thrombogenic and Inflammatory Reactions to Biomaterials in Medical Devices. *Front. Bioeng. Biotechnol.* **2020**, *8*, 1–18, doi:10.3389/fbioe.2020.00123.
3. Aparicio, H.J.; Benjamin, E.J.; Callaway, C.W.; Carson, A.P.; Cheng, S.; Elkind, M.S. V; Evenson, K.R.; Ferguson, J.F.; Knutson, K.L.; Lee, C.D.; et al. Heart Disease and Stroke Statistics-2021 Update A Report from the American Heart Association. *Circulation* **2021**, E254–E743, doi:10.1161/CIR.0000000000000950.
4. Cannegieter, S.C.; Rosendaal, F.R.; Briët, E. Thromboembolic and Bleeding Complications in Patients with Mechanical Heart Valve Prostheses. *Circulation* **1994**, *89*, 635–641, doi:10.1161/01.CIR.89.2.635.

5. Mehra, M.R.; Uriel, N.; Naka, Y.; Joseph C. Cleveland, J.; Yuzefpolskaya, M.; Salerno, C.T.; Walsh, M.N.; Milano, C.A.; Patel, C.B.; Hutchins, S.W.; et al. A Fully Magnetically Levitated Left Ventricular Assist Device — Final Report. *N. Engl. J. Med.* **2019**, *380*, 1618–1627, doi:10.1056/NEJMOA1900486.
6. Kuchinka, J.; Willems, C.; Telyshev, D. V.; Groth, T. Control of Blood Coagulation by Hemocompatible Material Surfaces—A Review. *Bioengineering* **2021**, *8*, 1–26, doi:10.3390/bioengineering8120215.
7. Vogler, E.A.; Siedlecki, C.A. Contact Activation of Blood-Plasma Coagulation. *Biomaterials* **2009**, *30*, 1857–1869, doi:10.1016/j.biomaterials.2008.12.041.
8. Furukawa, K.S.; Ushida, T.; Sugano, H.; Tamaki, T.; Ohshima, N.; Tateishi, T. Effect of Shear Stress on Platelet Adhesion to Expanded Polytetrafluoroethylene, a Silicone Sheet, and an Endothelial Cell Monolayer. *ASAIO J.* **2000**, *46*, 696–701, doi:10.1097/00002480-200011000-00009.
9. Ahmann, K.A.; Johnson, S.L.; Hebbel, R.P.; Tranquillo, R.T. Shear Stress Responses of Adult Blood Outgrowth Endothelial Cells Seeded on Bioartificial Tissue. *Tissue Eng.—Part A* **2011**, *17*, 2511–2521, doi:10.1089/ten.tea.2011.0055.
10. Jin, R.C.; Voetsch, B.; Loscalzo, J. Endogenous Mechanisms of Inhibition of Platelet Function. *Microcirculation* **2005**, *12*, 247–258, doi:10.1080/10739680590925493.
11. Dangas, G.D.; Weitz, J.I.; Giustino, G.; Makkar, R.; Mehran, R. Prostheticurrentc Heart Valve Thrombosis. *J. Am. Coll. Cardiol.* **2016**, *68*, 2670–2689, doi:10.1016/j.jacc.2016.09.958.
12. Wolfe, J.T.; Shradhanjali, A.; Tefft, B.J. Strategies for Improving Endothelial Cell Adhesion to Blood-Contacting Medical Devices. *Tissue Eng. Part B Rev.* **2022**, *28*, doi:10.1089/ten.teb.2021.0148.
13. He, W.; Butcher, J.T.; Rowlands, G.W.; Antaki, J.F. Biological Response to Sintered Titanium in Left Ventricular Assist Devices: Pseudoneointima, Neointima, and Pannus. *ASAIO J.* **2022**, *Publish Ah*, doi:10.1097/mat.0000000000001777.
14. Zapanta, C.M.; Griffith, J.W.; Hess, G.D.; Doxtater, B.J.; Khalapyan, T.; Pae, W.E.; Rosenberg, G. Microtextured Materials for Circulatory Support Devices: Preliminary Studies. *ASAIO J.* **2006**, *52*, 17–23, doi:10.1097/01.mat.0000189726.87077.ad.
15. Miyamoto, T.; Nishinaka, T.; Mizuno, T.; Tatsumi, E.; Yamazaki, K. LVAD Inflow Cannula Covered with a Titanium Mesh Induces Neointimal Tissue with Neovessels. *Int. J. Artif. Organs* **2015**, *38*, 316–324, doi:10.5301/ijao.5000423.
16. Robotti, F.; Franco, D.; Bänninger, L.; Wyler, J.; Starck, C.T.; Falk, V.; Poulikakos, D.; Ferrari, A. The Influence of Surface Micro-Structure on Endothelialization under Supraphysiological Wall Shear Stress. *Biomaterials* **2014**, *35*, 8479–8486, doi:10.1016/j.biomaterials.2014.06.046.
17. Gong, X.; Yao, J.; He, H.; Zhao, X.; Liu, X.; Zhao, F.; Sun, Y.; Fan, Y. Combination of Flow and Micropattern Alignment Affecting Flow-Resistant Endothelial Cell Adhesion. *J. Mech. Behav. Biomed. Mater.* **2017**, *74*, 11–20, doi:10.1016/j.jmbbm.2017.04.028.
18. Yoganathan, A.P.; Chaux, A.; Gray, R.J.; Woo, Y.R.; DeRobertis, M.; Williams, F.P.; Matloff, J.M. Bileaflet, Tilting Disc and Porcine Aortic Valve Substitutes: In Vitro Hydrodynamic Characteristics. *J. Am. Coll. Cardiol.* **1984**, *3*, 313–320, doi:10.1016/S0735-1097(84)80014-5.
19. Franco, D.; Milde, F.; Klingauf, M.; Orsenigo, F.; Dejana, E.; Poulikakos, D.; Cecchini, M.; Koumoutsakos, P.; Ferrari, A.; Kurtcuoglu, V. Biomaterials Accelerated Endothelial Wound Healing on Microstructured Substrates under Fl Ow. *Biomaterials* **2013**, *34*, 1488–1497, doi:10.1016/j.biomaterials.2012.10.007.
20. Stefopoulos, G.; Robotti, F.; Falk, V.; Poulikakos, D.; Ferrari, A. Endothelialization of Rationally Microtextured Surfaces with Minimal Cell Seeding Under Flow. *Small* **2016**, *12*, 4113–4126, doi:10.1002/smll.201503959.
21. Bachmann, B.J.; Giampietro, C.; Bayram, A.; Stefopoulos, G.; Michos, C.; Graeber, G.; Falk, M.V.; Poulikakos, D.; Ferrari, A. Honeycomb-Structured Metasurfaces for the Adaptive Nesting of Endothelial Cells under Hemodynamic Loads. *Biomater. Sci.* **2018**, *6*, 2726–2737, doi:10.1039/c8bm00660a.
22. Daxini, S.C.; Nichol, J.W.; Sieminski, A.L.; Smith, G.; Gooch, K.J.; Shastri, V.P. Micropatterned Polymer Surfaces Improve Retention of Endothelial Cells Exposed to Flow-Induced Shear Stress. *Biorheology* **2006**, *43*, 45–55.
23. Frendl, C.M.; Tucker, S.M.; Khan, N.A.; Esch, M.B.; Kanduru, S.; Cao, T.M.; García, A.J.; King, M.R.; Butcher, J.T. Endothelial Retention and Phenotype on Carbonized Cardiovascular Implant Surfaces. *Biomaterials* **2014**, *35*, 7714–7723, doi:10.1016/j.biomaterials.2014.05.075.
24. Ranjan, A.; Webster, T.J. Increased Endothelial Cell Adhesion and Elongation on Micron-Patterned Nano-Rough Poly(Dimethylsiloxane) Films. *Nanotechnology* **2009**, *20*, doi:10.1088/0957-4484/20/30/305102.
25. Wu, W.-T. Theoretical and Computational Studies on Thrombosis Growth and Multiphase Characteristics of Blood Flow, Carnegie Mellon University, 2015.